

4D Biofabrication of Mechanically Stable Tubular Constructs Using Shape Morphing Porous Bilayers for Vascularization Application

Mairon Trujillo-Miranda, Indra Apsite, Jose A. Rodríguez Agudo, Gissela Constante, and Leonid Ionov*

This study reports the fabrication of highly porous electrospun self-folding bilayers, which fold into tubular structures with excellent mechanical stability, allowing them to be easily manipulated and handled. Two kinds of bilayers based on biocompatible and biodegradable soft (PCL, polycaprolactone) and hard (PHB, poly-hydroxybutyrate) thermoplastic polymers have been fabricated and compared. Multi-scroll structures with tunable diameter are obtained after the shape transformation of the bilayer in aqueous media, where PCL-based bilayer rolled longitudinally and PHB-based one rolled transversely with respect to the fiber direction. A combination of higher elastic modulus and transverse orientation of fibers with respect to rolling direction allowed precise temporal control of shape transformation of PHB-bilayer – stress produced by swollen methacrylated hyaluronic acid (HA-MA) do not relax with time and folding is not affected by the fact that bilayer is fixed in unfolded state in cell culture medium for more than 1 h. This property of PHB-bilayer allowed cell culturing without a negative effect on its shape transformation ability. Moreover, PHB-based tubular structure demonstrated superior mechanical stability compared to PCL-based ones and do not collapse during manipulations that happened to PCL-based one. Additionally, PHB/HA-MA bilayers showed superior biocompatibility, degradability, and long-term stability compared to PCL/HA-MA.

According to the World Health Organization, during the last century, the failure of blood vessels associated with CVD has become around 30% of the leading causes of death worldwide.^[2,3] One possible solution for the replacement of non-functional blood vessels with a diameter >8 mm is nonresorbable blood vessel grafts made of synthetic non-biodegradable polymers such as polyethylene terephthalate (trade name Dacron) and polytetrafluoroethylene. Nonetheless, despite substantial advances in the successful bypassing of injured vessels, it has been reported that ≈70%–80% of these often fail due to thrombus formation.^[4–6]

More advanced approaches for the fabrication of blood vessels are based on tubular scaffolds with incorporated cells. Thereupon, 3D bioprinting/biofabrication has focused on developing artificial vessels that mimic the circulatory system's anatomical properties.^[7–11] Nonetheless, the main drawbacks faced by the technique include the limited resolution achieved during the fabrication of small narrow tubular structures (<6 mm) and perilous shear forces

generated upon fabrication of thicker arteries or veins.^[12,13] Moreover, when a supporting layer made from a fast-degradable material is often used to preserve the final tube-like structure, its removal remains the main challenge due to the high softness and brittleness of the main 3D printed hydrogels on top of this. Furthermore, cell seeding in tubular structures postprinting becomes problematic due to rapid sedimentation and poor cell distribution.


In contrast to 3D printing, electrospinning has shown advances and gained considerable attention for fabricating highly porous and mechanically as well as structurally anisotropic scaffolds with high versatility to recreate an in-vitro extracellular matrix (ECM) model.^[14–17] There are various ways to achieve tubular structures using electrospinning. The first possibility is the use of a cylindrical mandrel. For instance, Xian et al.^[18] and Javanmard et al.^[19] have manufactured electrospun polycaprolactone (PCL) bi- and trilayers, where fibers were slowly collected on top of a cylindrical mandrel at low speed. However, even though the method is relatively simple, it does not offer a wide variety of tube diameters or high fiber alignment along the main axis.

1. Introduction

Cardiovascular diseases (CVD) have been considered since 1989 as one of the most hazardous causes of annual mortality.^[1]

M. Trujillo-Miranda, I. Apsite, G. Constante, L. Ionov
Faculty of Engineering Sciences and Bavarian Polymer Institute
University of Bayreuth
Ludwig Thoma Str. 36A, 95447 Bayreuth, Germany
E-mail: leonid.ionov@uni-bayreuth.de

J. A. R. Agudo
Anton Paar Germany GmbH
Hellmuth-Hirth-Str. 6, 73760 Ostfildern-Scharnhause, Germany

 The ORCID identification number(s) for the author(s) of this article can be found under <https://doi.org/10.1002/mabi.202200320>

© 2022 The Authors. Macromolecular Bioscience published by Wiley-VCH GmbH. This is an open access article under the terms of the Creative Commons Attribution License, which permits use, distribution and reproduction in any medium, provided the original work is properly cited.

DOI: 10.1002/mabi.202200320

These issues of 3D printing and electrospinning using rod-like templates are addressed by 4D biofabrication methods, which assume shape-transformation of flat mono- or bilayers with homogeneously adhered different kinds of cells.^[13,20,21] The shape transformation occurs due to differences in polymers' swelling properties forming bilayers or gradients of swelling degree formed inside a monolayer. The shape transformation can occur in response to various stimuli: temperature, aqueous medium, etc.^[22,23] Besides that, 4D biofabrication does not require very high resolution that eliminates the need for high shear stresses, which are usually applied during scaffold fabrication using traditional approaches such as 3D printing, which negatively affect cell viability.^[18–20]

The creation of vascular structures using 4D biofabrication has shown great potential in the latest years.^[17,24–26] For instance, Yuan et al.^[26] produced spin-coated polydimethylsiloxane (PDMS) membranes that, after being cured, lead to thicker multi-wall tubular constructs. Nevertheless, the spontaneous transformation was only possible due to stress differences previously induced through a mechanical stretcher. On the other side, Zhan et al.^[24] 3D printed biopolymer sheets that actuated upon swelling gradient, resulting in tubular constructions ranging between 20 and 500 μm , with high internal wall flexibility and integrity for benefiting the replacement of microvascular tissues. However, the high smoothness and low diffusion of nutrients due to the small mesh size of 3D printed hydrogels often hinder mechanical stability, cellular migration, and proliferation. Moreover, hydrogels lack important guidance cues and thus have a low resemblance to the anisotropic nature of the ECM.^[27] Thus, in other reports electrospinning is used to form 4D biofabricated tubular structures for blood vessel formation.^[17] Nonetheless, fibrous monolayers, comprising PCL and poly (lactic-co-glycolic acid) random electrospun fibers, only actuated due to mechanical stretching produced by external nonbiodegradable PDMS strips – external force shall be applied. Besides that, electrospun scaffolds depicted a low degree of degradation due to the synthetic nature of studied polymers. Self-actuated transformation can be introduced using bilayer systems consisting of polymers with different swelling properties. Fabrication of fibrous self-folding electrospun bilayers has shown significant improvements like fast actuation rate, fast perfusion of media, uniform cell seeding, and cell guidance in the last couple of years.^[28] Usually, these systems have been formed using PCL as one of the components, though PCL is easily processible polymer, PCL fiber orientation in scaffold highly depends on scaffolds shape and size.^[29,30]

Another drawback of PCL is its low elastic modulus that often leads to collapse of self-folded structures when they are removed from aqueous media. One possible solution for this problem is the use of stiffer biodegradable polymers with a high glass transition temperature (T_g). The elastic modulus of such polymers is closer to that of collagen nanofibers, and they provide better stability to the scaffold. Thereby, biodegradable polyhydroxyalkanoates (PHAs) have often been proposed to fabricate fibrous scaffolds due to their higher stiffness, high biocompatibility, thermoplasticity, and low level of immune rejection. Polyhydroxybutyrate (PHB) has been thoroughly studied and considered the standard PHA; PHB is a biodegradable polyester obtained from bacterial fermentation, whose physical and mechanical properties can easily be tuned during spinning.^[31–33] Furthermore, elec-

trospun PHB fibers have depicted non-toxicity, slow hydrolysis rate, and adjustable porous morphology.^[34,35] Compared to PCL, which is usually synthesized in the laboratory,^[36] naturally derived PHB has led to the fabrication of thin nanoporous scaffolds with a higher surface-to-volume ratio, making it suitable for supporting the proliferation of different cell lines.^[37] Both materials used for passive layer formation are FDA-approved.^[30,38–41] Besides that, in both systems, hyaluronic acid (HA) was used as the second layer – active layer, which is FDA (food and drug administration) approved and widely used for tissue engineering applications.^[42–44]

Therefore, in this study, we are introducing, highly aligned and self-actuating electrospun bilayers with high stability after various manipulations in and out of aqueous media for potential vascular graft fabrication. Furthermore, we compared properties of PHB and PCL-based scaffolds (mechanics, biocompatibility, self-actuation), examining both materials used in the bilayer system to overcome previous challenges associated with poor stability related to low modulus and hard to control main fiber alignment through tubular structure.^[17,30] Using PHB based system we have achieved high degree of fibers alignment and transverse orientation with respect to the main axis of formed tubes which could allow efficient reinforcement in a transverse direction and prevents collapse of tubes due to capillary forces for further investigations. In this study endothelial cell adhesion and proliferation have been investigated to prove biocompatibility of constructs for blood vessel formation.

2. Results and Discussion

This work is focused on the fabrication of self-actuating electrospun bilayers with potential properties for replacing blood vessels. Electrospinning was utilized to fabricate the first layer formed by PCL (9 wt.%, 0.6 mL h^{-1} , 6000 rpm) or PHB fibers (15 wt.%, 1 mL h^{-1} , 3000 rpm) (Figure 1a,b). A higher concentration of PHB was needed to form fibers – more diluted PHB solutions did not form fibers. The zero shear viscosities of both polymer solutions are similar and are in the range of a few mPa·s. The similar viscosity at considerably different concentrations means that the molecular weight of PHB is lower than that of PCL. At a high shear rate, the viscosity of PHB solution decreases to the level of that of PCL solution (Figure S1e, Supporting Information).

Applying an electric field to extruded solutions resulted in the formation of multiple jets, which dried out and formed fibers with different diameters: $2.8 \pm 0.4 \mu\text{m}$ and $4.9 \pm 0.5 \mu\text{m}$ for PHB and PCL, respectively (Figure S1a–c, Supporting Information). The production rate of PHB and PCL fibers corresponding to conditions of the experiment are 150 mg h^{-1} and 54 mg h^{-1} , respectively. Interestingly, while the viscosity of PHB solution and its concentration is higher than those of PCL, the diameter of produced fibers is smaller. The lower molecular of PHB could be the origin of the smaller diameter of PHB fibers. Due to the lower molecular weight of PHB, viscosity of its solution increases more slowly upon evaporation of the solvent than viscosity of PCL solution does. As result, PHB fibers can be stretched more strongly by electric field than PCL fibers.

The use of an ultra-high-speed rotating drum allowed a very high degree of fiber alignment ranging among 50%–60% and

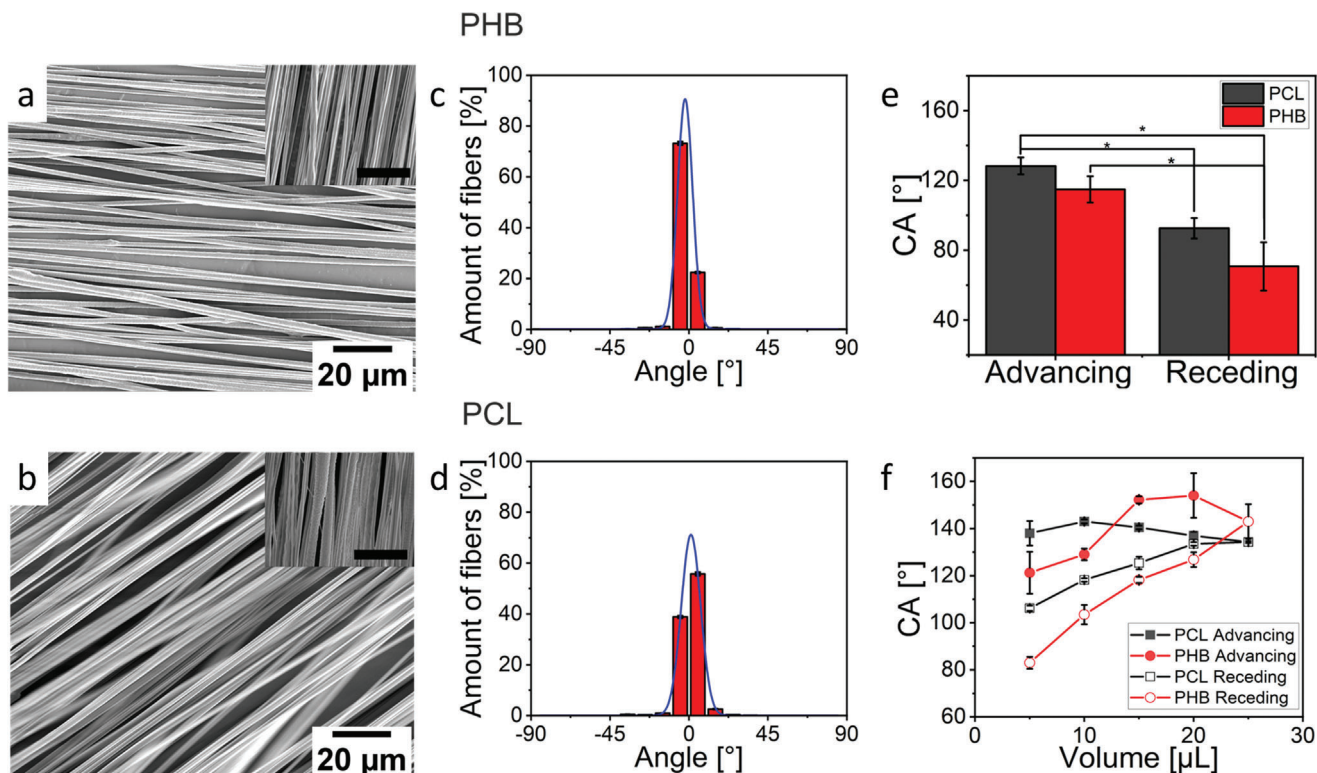


Figure 1. Properties of electrospun PCL and PHB fibers: SEM (scanning electron microscopy) images of highly aligned PCL a) and PHB b) fibers (insert scale: 5 μm); estimated alignment of PCL c) and PHB d) fibers; e) average contact angle (CA) measurements (*, $p < 0.05$); and f) hysteresis of advancing and receding contact angle measurements of PCL and PHB mats.

70%–80%, and for PCL and PHB, respectively (Figure 1c–d). Important, highly aligned PHB fibers could be produced at 3000 rpm (tangential speed is 8.5 m s^{-1}), while fabrication of highly aligned PCL fibers required two times the collection speed used for PHB (6000 rpm, tangential speed is 17 m s^{-1}). The need for lower rotation speed for fabrication of aligned PHB fibers is most probably related to its lower molecular weight – viscosity increases slower with solvent evaporation in comparison to PCL solutions. It was observed that the high take-up speed led to a significant reduction in the fiber diameter of both polymers ($1.3 \pm 0.2 \mu\text{m}$ and $1.4 \pm 0.2 \mu\text{m}$ for PCL and PHB, respectively) in contrast with fibers produced using stationary collector ($2.8 \pm 0.4 \mu\text{m}$ and $4.9 \pm 0.5 \mu\text{m}$, for PHB and PCL, respectively) (Figure S1c). This means that not only electrostatic forces stretched droplets out of the multiple jets that resulted in the formation of the aligned fibers, but also the collector led to a considerably higher degree of stretching, mechanically improving the alignment of PHB in comparison with PCL (Figure 1d,c). This means that the use of more concentrated solutions of polymers with lower molecular weight in combination with high rotation speed of collector allows high production rate of fibers.

We can expect that the smaller diameter of the obtained fibers should also be advantageous for cells adhesion – as they prefer to adhere to thin fibers with diameters ranging between 1 and $10 \mu\text{m}$ that is the diameter of collagen fibers. Besides that, high alignment is expected to guide the alignment of cells. It is also important that in this experiment, we were able to achieve a very high degree of alignment of PHB fibers, which was not previ-

ously possible (30%–35%)^[45,46] due to the brittleness of the fibers obtained associated as well with the low concentration of the polymer solution.

We studied the properties of obtained electrospun mats. The thermal analysis of both electrospun monolayers was performed using DSC (differential scanning calorimetry) measurements at a rate scan of 1 K/min (Figure S1d, Supporting Information). PHB fibers depicted a higher melting ($175 \text{ }^\circ\text{C}$) and crystallization temperature ($80 \text{ }^\circ\text{C}$) in contrast with PCL fibers ($60 \text{ }^\circ\text{C}$ and $27 \text{ }^\circ\text{C}$). Larger hysteresis in the case of PHB means that crystallization is hindered due to its T_g around $4\text{--}5 \text{ }^\circ\text{C}$ at ambient conditions.^[47] The degree of crystallinity was estimated to be ≈ 56 and 37% for PHB and PCL, respectively. Thus, both polymers can be considered semicrystalline.

Contact angle (CA) measurements were performed to quantify the hydrophobicity of both electrospun mats. Surprisingly, even when both polymer mats exhibited similar wetting properties during advancing contact angle measurements, which in both cases was above 120° (Figure 1e,f), measurements of receding contact angle showed a considerable difference in wetting properties – PHB shows receding contact angle around 70° , being more hydrophilic than PCL ($\approx 93^\circ$) (Figure 1f). We made reference measurements of CA on pure films and found that CA was way lower on simple static conditions achieving values $\approx 82^\circ$ and 78° for PCL and PHB, respectively (Figure S2, Supporting Information). Thus, due to roughness, e-spun mats have poor wetting properties (high values of advancing contact angle compared to flat polymer films).^[48] We believe that the difference in

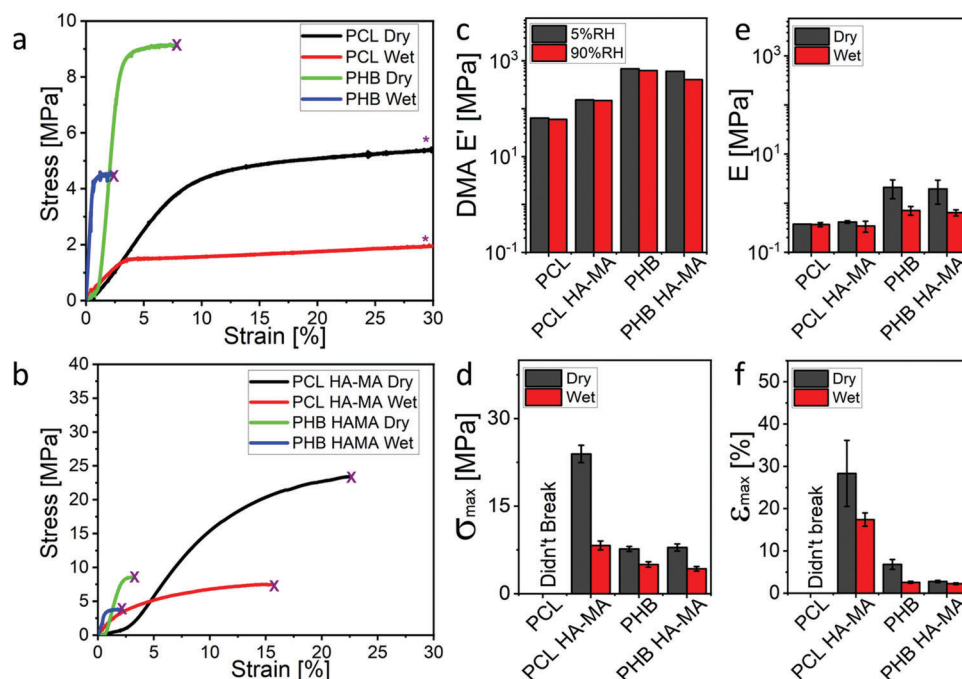


Figure 2. Mechanical properties of electrospun PCL, PHB mono and PCL/HA-MA, PHB/HA-MA bilayers: Stress-strain curves of PCL, PHB mats a) and PCL/HA-MA, PHB/HA-MA bilayers b) (x, Samples were broken, *, samples were not broken); c) dynamic mechanical analysis (DMA) of electrospun mono and bilayers d) ultimate tensile strength; e) Young's modulus from tensile test; and f) elongation at break of PCL, PHB monolayers and PCL/HA-MA and PHB/HA-MA bilayers.

morphology of PHB and PCL electrospun mats (Figure S1a,b, Supporting Information) is the reason for the difference in receding angle because the chemical structure of polymers is similar and contact angles of flats surfaces are nearly identical. There are, however, no suitable models allowing the prediction of wetting of such complex and irregular surfaces as nanofibrous mats.

Mechanical properties of pure polymers were evaluated by performing tensile tests of rectangular e-spun mats (longitudinal direction) at room temperature in both dry and wet states. Tensile tests demonstrated that PHB fibers are much stiffer than PCL fibers – their elastic modulus is two orders of magnitude higher (2.1 MPa) than PCL (0.38 MPa). One needs to understand that obtained values are much lower than bulk polymers due to the porous structure of the fibrous mat. PHB is also much more brittle than PCL, and the maximal elongation (6.9 MPa) at which polymer break depends on the environment. The brittleness of PHB is due to high T_g (Figure S1d, Supporting Information), which is because of hindered rotation around the C-C bond of the main polymer chain. As a result, the maximal strain at the break was inferior (2-6%) in contrast with PCL (>30%) (Figure 2f).

Wet conditions had almost no effect on the elastic moduli of both polymers (Figure 2e). While the elastic modulus of both polymers is independent of the environment, the yield stress, stress during necking, and elongation at the break are reduced in a wet environment compared to a dry one. This effect can be explained by the fact that necking is associated with the formation of multiple microcracks that becomes easier upon reducing the interfacial tension between polymer and environment.

Next, we fabricated bilayers and studied their mechanical properties. For subsequent fabrication of PCL/HA-MA and PHB/HA-

MA bilayers, the HA-MA layer (the active component of bilayer) was spun on top of aligned PCL or PHB fibers. HA-MA fiber diameter was $\approx 0.3 \pm 0.06 \mu\text{m}$. The orientation of HA-MA fibers is not relevant because cells would not be in direct contact with it, and their proliferation should not be affected. As one of the main components of the ECM, which is responsible for turgor pressure, HA-MA possesses extensive swelling properties upon media immersion that often interfere with cell adhesion.^[49] The swelling of HA-MA is the driving force for the shape transformation of bilayers.

To understand each polymer's degree of contribution to the bilayer's mechanical properties, bilayers were subjected to tensile tests using the previously described conditions (wet and dry states). In the dry state, both polymers contribute to mechanical properties. In contrast, in the wet state, when HA-MA is swollen, only hydrophobic polymers (PCL and PHB) shall determine the mechanical properties of the bilayers (Figure 2b). Experimental observations support this assumption: elastic modulus PCL/HA-MA decreases from 0.42 MPa in the dry state down to 0.34 MPa in wet conditions, and elastic modulus of PHB/HA-MA decreases from 1.93 MPa in the dry state down to 0.64 MPa in a wet state (Figure 2e). We observed that bilayers rupture at smaller elongation than pure hydrophobic polymers in dry and wet states. We believe that this effect arises due to the presence of swelling of HA-MA fibers, PCL and PHB fibers are pushed apart, leading to a lower maximal strain (Figure 2f).

Next, pure PCL and PHB mats, as well as PCL/HA-MA and PHB/HA-MA bilayers, were subjected to DMA measurements using a modular humidity generator (MHG 100 proUmid, Germany) (Figure 2c and Figure S3a–d, Supporting Information). As

scaffolds are intended to recreate conditions found within the human body, thus the main aim was to see the effects of temperature and humidity simultaneously on mechanical properties. As expected, the humidity did not significantly impact pure e-spun PCL and PHB mats (Figure 2c and Figure S3a,b, Supporting Information) due to their inherent hydrophobicity. Besides that, compared to large deformation analyzed during tensile testing measurements, the elastic moduli obtained for these was almost three times higher, ranging from 60 and 650 MPa for PCL and PHB, respectively. The applied forces were fixed during DMA, and the samples went over their linear viscoelastic region at a maximum amplitude of 0.1% strain. Contrarily to samples subjected to tensile test where the slope was above 5%, we can conclude that the e-spun mats were never subjected to their maximum displacement during DMA measurements, and irreversible deformation never occurred.

Next, both bilayers were subjected to the same DMA measurements to check whether HA-MA contributes to a reduction of the mechanical properties (Figure 2c and Figure S3a–d, Supporting Information). Irrespective of the fact that there was a slight drop in E' marked in Figure S3c,d, Supporting Information for both bilayers, it was determined that the application of high humidity did not lead to important changes in the mechanics of the materials (Figure 2c). This means that HA-MA did not have any significant contribution, and the hydrophobic character of both PCL and PHB mainly determined the mechanics.

Shape transformation into the tubular scroll-like structure of PCL/HA-MA and PHB/HA-MA bilayers was studied in different aqueous media (MilliQ-water, PBS, and HUVECs media). Fast formation of scroll-like structures occurred between 1 and 2 min after bilayer sheets were immersed in media (Figure 3a,b, and Videos S1 and S2, Supporting Information). The folding can be controlled by applying a weight – a Teflon ring placed on bilayers prevents folding and folding continues once removing the ring after 1 h. It was found out that the folding of PHB-based bilayer was not affected by exposure to weight and folding rate, contrary the amplitude of PCL-based one, was reduced after this exposure to weight.

Interestingly, folding of PHB/HA-MA always occurred perpendicular to the main fibers axis, resulting in tube formation with fibers oriented perpendicular to its main axis, leading to stable structures that kept their shape in both dry and wet states. In contrast, folding PCL/HA-MA bilayers also depicted an interesting behavior – biaxial handscroll formation^[50] due to simultaneous folding starting from two opposite sides. Folding happened parallel to the main axis of the fibers, and the latter was oriented parallel to the main axis of the tube. Thus, we can expect that transverse aligned PHB fibers reinforce the tube against transverse deformation, resulting in tubes collapse due to capillary forces. PCL fibers are not able to do this due to longitudinal orientation with respect to the main tube axis.

The effect of overall thickness and the passive-active ratio on the diameter of formed tubes (Figure 3c,d) was also studied. It was observed that increasing the thickness and the ratio between hydrophilic and hydrophobic polymers of the electrospun bilayers headed to a bigger diameter, wherein PHB/HA-MA and PCL/HA-MA were ranging 1–14 mm and 2.6–13 mm, respectively. This agrees qualitatively with Timoshenko's equation, where it is stated that the higher the ratio between both layers, the

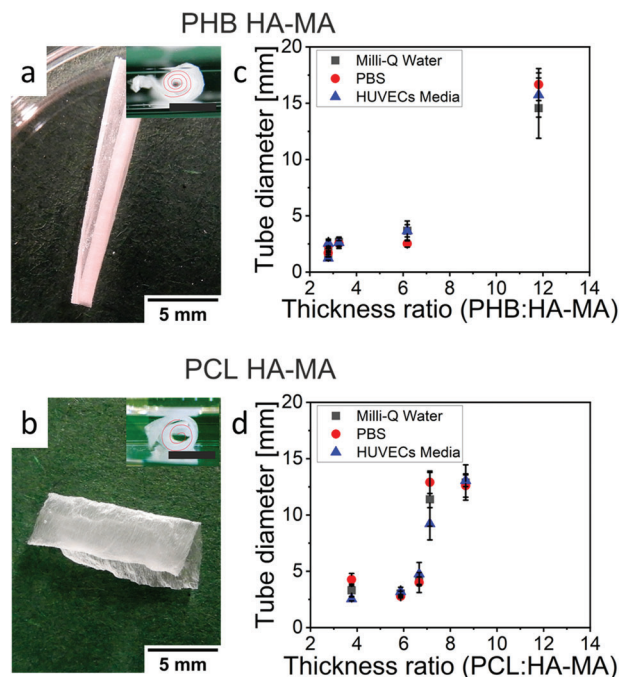


Figure 3. Shape transformation of PCL/HA-MA and PHB/HA-MA electrospun bilayers: folded PCL/HA-MA a) and PHB/HA-MA b) tubes (insert: tube cross-sections, scale bar: 3 mm); thickness ratio influence on the final tube diameter of PCL/HA-MA c) and PHB/HA-MA d) bilayers.

higher the curvature's radius.^[51] This effect has also been previously discussed by Apsite et al.^[29,30] It was claimed that larger tube diameters could be achieved by playing with the ratio between the thickness of hydrophobic and hydrophilic layers.

The tube diameter of rolled scaffolds was found to be nearly independent of the concentration of Ca^{2+} ions in the range of 0–1 M (Figure S4, Supporting Information). We observed that the inner diameter could be slightly tuned by increasing Ca^{2+} concentration, although complete unfolding never occurred (Video S3, Supporting Information), which agrees with the results previously obtained.^[30] Thus, contrary to recently studied PCL/AA-MA structures,^[29,38] the main diameter of HAMA-based tubes remained nearly insensitive to the concentration of Ca^{2+} . Thus, the tube diameter can be adjusted solely by varying the thickness ratio of both layers and the thickness of the bilayer.

Real-time degradations studies were conducted on electrospun PCL and PHB fibers and PCL/HA-MA and PHB/HA-MA folded and nonfolded bilayers for 4 weeks. As expected, due to studies previously conducted,^[30] PCL slowly degraded during 4 weeks of incubation (Figure 4a,d and Figure S5a,e,i, Supporting Information) although its surface becomes rougher due to the formation of cavities. The surface porosity of PCL increased by $\approx 67\%$, showing a rougher surface in the last week (Figure 4d) contrary to initial porous morphology ($\approx 32\%$) before degradation (Figure 1b and Figure 4a). In contrast to this, PHB fibers depicted a more complex behavior. Smooth electrospun fibers started to get cracked after one week of incubation (Figure S6c, Supporting Information), and the number of cracks started to progressively increase throughout the incubation period (Figure S6g,h, Supporting Information). Finally, after last week, most of the fibers were

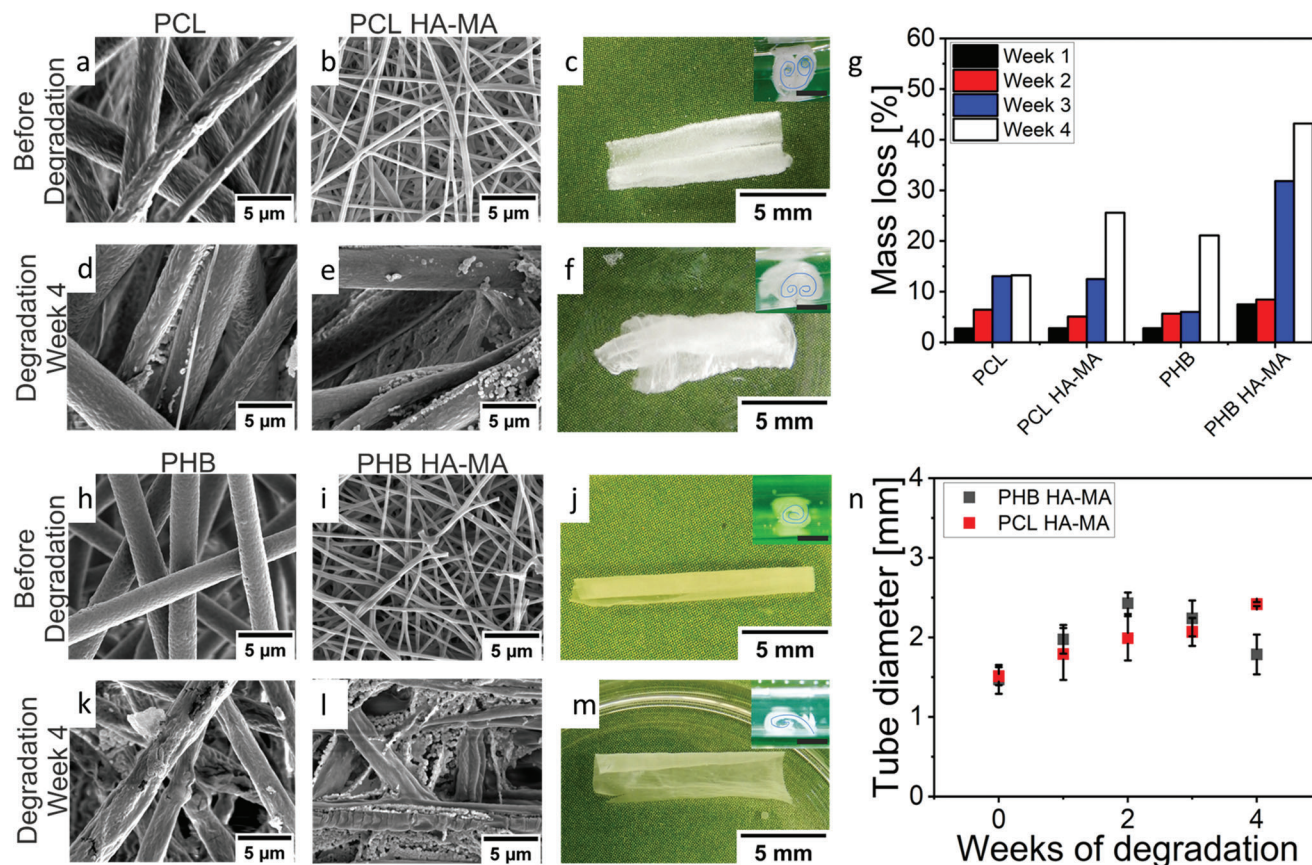


Figure 4. Degradation behavior of electrospun mono and bilayers: morphology of electrospun PCL fibers, PCL/HA-MA bilayer and folded PCL/HA-MA bilayer before a–c) and after 4 weeks of degradation d–f) (insert: tube cross-sections, scale bar: 3 mm scale); g) mass loss of electrospun PCL and PHB fibers and PCL/HA-MA and PHB/HA-MA bilayers; morphology of electrospun PHB fibers, PHB/HA-MA bilayer and folded PHB/HA-MA bilayer before h–j) and after 4 weeks of degradation k–m); n) effect of degradation over final tube diameter of PCL/HA-MA and PHB/HA-MA tubular scaffolds.

broken. Those that remained partially intact had several voids and presented bottle-neck-like morphology (Figure 4k), depicting a bulk erosion behavior, where both the surface and the inside of the fibers were simultaneously getting degraded. Mass loss studies confirmed all the morphological changes (Figure 5g). PCL effectively lost 13% of its mass, whereas PHB mass loss reached (Figure 4k) 20%. Thus, both PCL and PHB electrospun mats are biodegradable, while PHB degrades faster. PCL/HA-MA bilayers showed complete degradation of HA-MA fibers after one week of incubation (Figure S5b, Supporting Information). Also, the number of cavities on the PCL fibers increased, and after the fourth week, the final morphology was similar to that of single PCL fibers (Figure 4e). Folded PCL/HA-MA bilayers showed a visible effect of degradation on the general shape of tube-like scaffolds, the tube-like constructions slowly unfolded after the second week (Figure S6b, Supporting Information), leading to a partially overlapping tube. Nonetheless, we observed that after the last week of incubation (Figure 4c), unconstrained tubular scaffolds retained their tubular structure, but inner diameter increased from 1.5 up to 2.4 mm (Figure 4n). The degradation behavior of PHB/HA-MA is different from that of PCL/HA-MA. We could see how HA-MA fibers started to slowly degrade on week one, leading to morphological changes in the PHB fibers. We noticed dur-

ing SEM that even in the dry state, HA-MA fibers could dissolve and partially get embedded within PHB. Therefore, instead of being eliminated during degradation studies, as in PCL/HA-MA (Figure S5b, Supporting Information), these seemed to dissolve and form some imprints on the PHB mat (Figure S5d, Supporting Information). These imprints were more pronounced and spread along with the mat during the incubation period, fostering a faster crack formation along the PHB fibers (Figure S6h,i, Supporting Information). We also observed formation of particles with a size $\approx 1 \mu\text{m}$. The particles were observed in the case of both mono- and bilayers that means that their origin is most probably the hydrophobic polymers. It is known that the amorphous part of polymers degrades faster that allows us to speculate that the particles are most probably the domains with higher crystallinity. Eventually, after four weeks, HA-MA formed a coating along with the mat. Mass loss studies showed that PCL/HA-MA by its side reached around 25% of loss that could be correlated to the complete elimination of HA-MA and a slight reduction in the PCL fibers. At last, the degradation of the PHB/HA-MA bilayer was the most significant, with a weight loss of 43%. The rapid degradation rate of the PHB/HA-MA bilayer could have been triggered due to fast HA-MA elimination. The remaining imprints boosted faster-cracking formation on top of the PHB fibers, leading to a

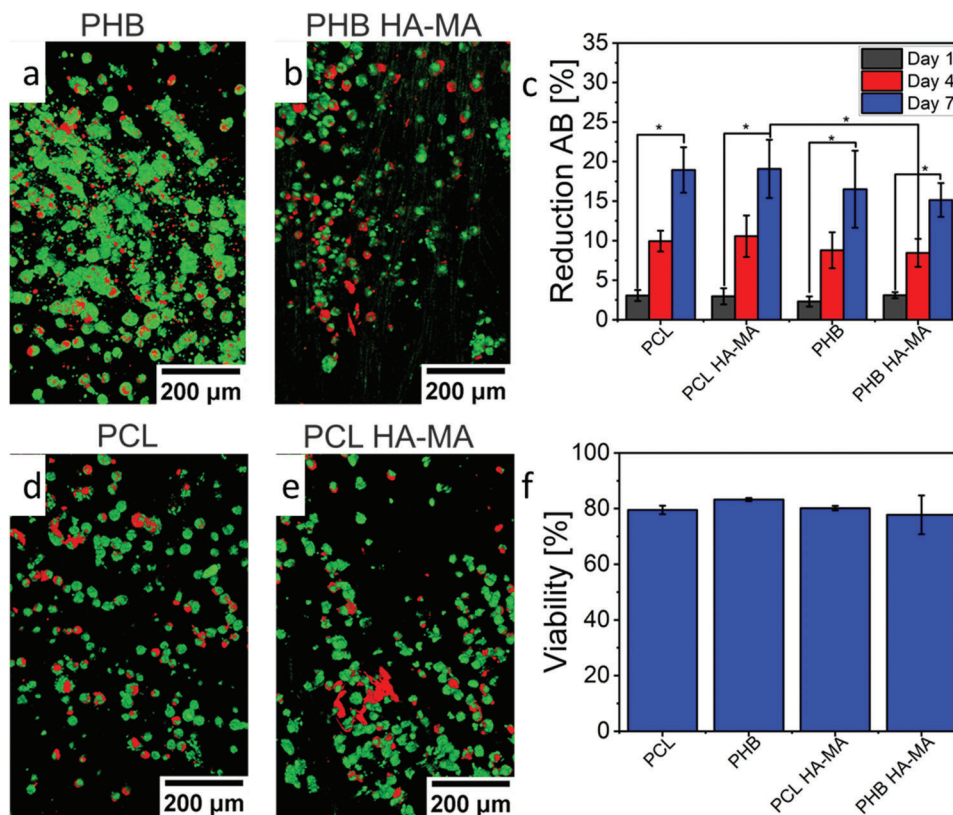


Figure 5. Cell culture studies of HUVECs on electrospun mono and bilayers: live dead assay of HUVECS on PCL a) and PCL/HA-MA b) scaffolds (Live: green and dead: red); c) HUVECs proliferation on electrospun mono and bilayers after 1, 4 and 7 days of cultivation (*, $p < 0.05$); live dead assay of HUVECS on PHB d) and PHB/HA-MA e) scaffolds; f) cell viability after seven days of cultivation.

superior mass loss than PCL/HA-MA mats. In conclusion, these experiments showed that mono – as well as bilayer scaffolds, are biodegradable.

HUVECs (human umbilical vein endothelial cells) were cultured on top of electrospun mats to prove the biocompatibility of individual polymers and bilayers (Figure 5). After 1 day of cultivation, we observed similar cell proliferation on both mono and bilayers (Figure 5c). The cell interaction improved during incubation, and proliferation rose, achieving around 18%–20% on day 7 for all scaffolds. The significant difference among bilayers is noteworthy, wherein PCL/HA-MA was slightly higher than PHB/HA-MA due to the apparent slow elimination of HA-MA fibers. The cell viability was ascertained after 7 days using a live/dead assay (Figure 5a-1 and d,e, Figure S7, Supporting Information). Results showed viability above 80% for all scaffolds with no statistical difference between them (Figure 5f). Despite the non-existing difference among the mats, the number of dead cells was more marked on the PCL and PCL/HA-MA fibers (Figure 5a,b). Contrary, PHB seemed to offer better anchoring points for the cells (Figure 5d,e), and as a result, these were able to spread along the fibrous scaffolds and remained alive. Thus, all the scaffolds proved to be biocompatible and support cell growth.

The alignment of HUVECs was studied after days 4, 7, and 14 of cultivation. It was found that independent of the substrate (Figure 6 m,n,o,p), the degree of alignment of cell nuclei decreases with time. Endothelial cells can easily change their mor-

phology upon high confluency;^[52] this modifies their orientation, and nuclei tend to rearrange randomly. Nevertheless, the decrease in alignment degree of HUVECs with time is not expected to be a problem for applying tubular structures within bioreactor/animal because they tend to align under the influence of shear forces generated by a fluid flowing through the vascular conduit.

Time evolution of the fraction of the surface of electrospun mats covered with cells has a different character depending on mats. The initial fraction of PHB surface covered by cells is the largest amount of all other samples, and it decreases with the time approaching 40%–50%. Fraction of PCL surface covered by cells did not change with time and always remained 40%–50%. The initial fraction of bilayers surface covered by cells is low and increases with time, approaching 40%–50%. The difference in the time evolution of the fraction of surface of mono- and bilayers covered with cells clearly show a negative effect of the hydrophilic HA-MA layer on cell adhesion, which gets improved may be due to partial degradation of HA-MA. We can hypothesize that two weeks were not enough to cover 100% of the electrospun mats and endothelial cell adhesion could be improved by using laminin or decorin coating.^[53–55] Some studies^[56,57] revealed that the minimum time for achieving complete reendothelialization was ≈ 4 weeks. Besides that, the use of vascular endothelial growth factors (VEGF) together with neuropilin-1, which serves as co-receptor for VEGF and regulates VEGF-dependent

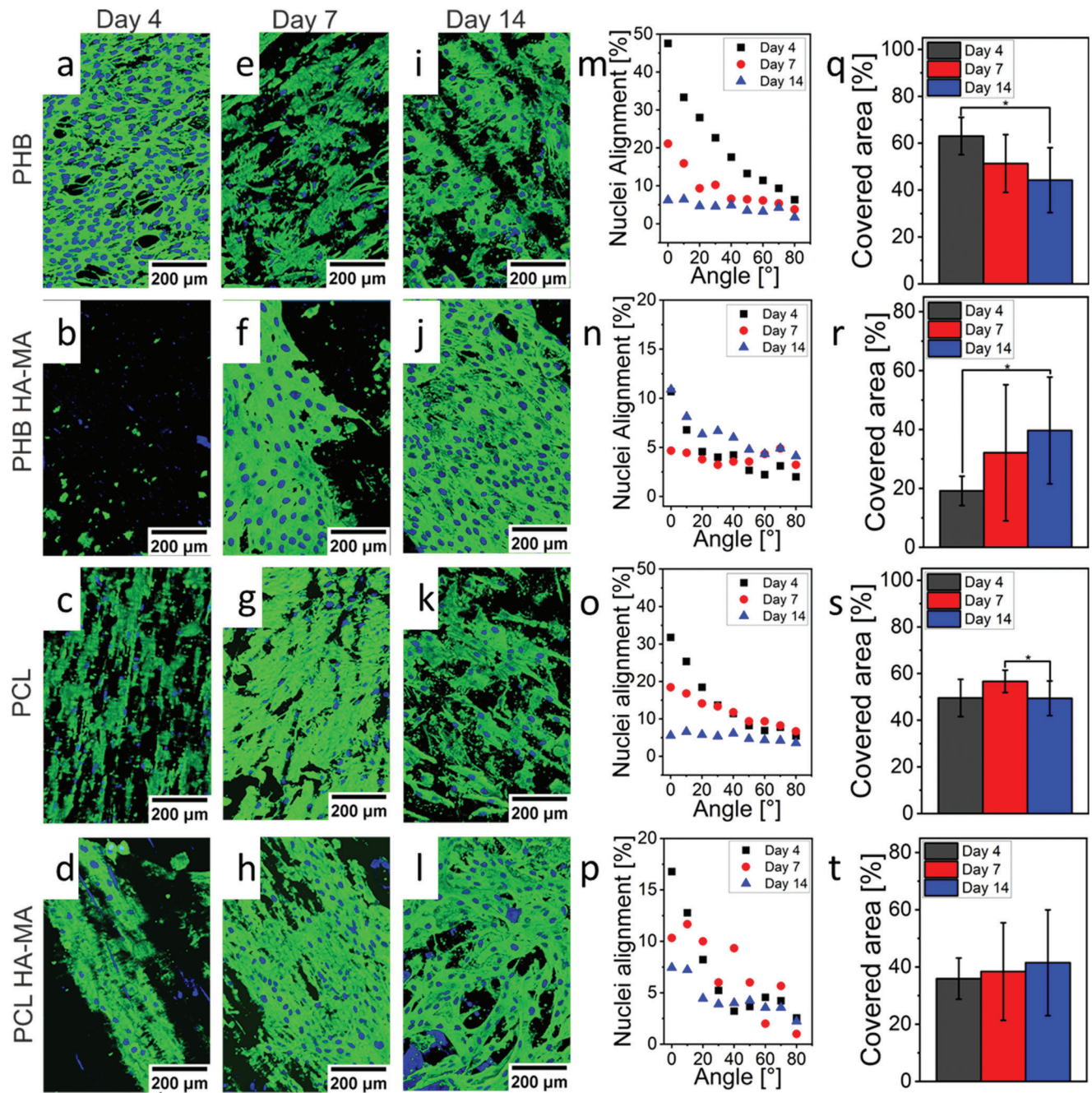


Figure 6. Cell alignment and coverage of HUVECs on electrospun mono and bilayers: confocal images of HUVECs on electrospun mats on day 4 a,b,c,d), day 7 e,f,g,h), and day 14 i,j,k,l) (actin filament: green and nuclei: blue); percentage of nuclei alignment m,n,o,p); and area covered by HUVECs q,r,s,t) (*, $p < 0.05$).

angiogenesis, could be a good option to improve cell growth and vascularization.^[54,57] The most important observation is that the surface coverage (40-50%) after two weeks is independent of the kind of bilayer.

Finally, we fabricated an electrospun artificial vascular graft by using self-actuating bilayers. HUVECs were cultured prior to self-folding on top of the electrospun sheets. To restrict the folding of the bilayer, Teflon rings were used. After <1 h, we noticed

that the self-folding of PHB/HA-MA bilayers was not affected, and structures were stable for 14 days of cultivation. Whereas PCL/HA-MA scaffolds morphology was altered by long restriction – either they took more time to fold and needed to be shaken or aided with tweezers. Moreover, tube diameter was also partially influenced; one of the bilayers only folded from one side and tended to unfold while incubation time passed. The stretching of PCL fibers could explain this upon swelling of HA-MA.

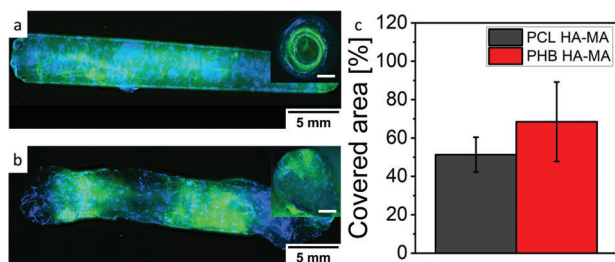


Figure 7. Fabrication of shape-morphing vascular grafts: fluorescent images of cultured HUVECs within self-folded PCL/HA-MA a) and PHB/HA-MA b) electrospun bilayers (actin filament: green and nuclei: blue; insert: tube cross-sections, scale bar: 3 mm scale); and c) a percentage of area covered by HUVECS after 14 days of cultivation.

The structure was already too soft (T_g of PCL is very low, and a relatively fast stress relaxation process may happen), and the weight of the ring seemingly hampered the formation of the roll structure.

After 14 days of cultivation, the artificial vessels were imaged, and we could observe a high number of cells within both scaffolds, represented by staining of their bodies. The PHB/HA-MA bilayers were more stable during imaging in and out of the liquid media and tended to retain their tubular structure for a longer time (Figure 7b). In contrast, PCL/HA-MA conduits collapsed a few seconds after being removed from the medium and formed a dog bone-like structure (Figure 7a). The cross-section of both conduits can also support these findings. PHB/HA-MA conduits showed a more defined scroll-like section filled with cells on different levels (Figure 7b). The inner diameter of tube shown in Figure 7b are 2.4 (left), 2.3 (center) and 2.3 mm (right). Unfortunately, for the PCL/HA-MA conduits, the lack of resistance made it hard to image cross-section properly and distinguish whether cells migrated along with the sheet or remained on the main surface (Figure 7a). We theorize that the softness of PCL and longitudinal orientation of fibers could have been the main factor why the bilayers could not retain their shape for a longer time. Furthermore, we also noticed that after being collected on the drum, PCL fibers tended to relax slightly, leading to rearrangement of the polymer's chains, and consequently generating possible conformational changes in the main shape of the fibers. In contrast, PHB fibers always retained their direction and shape, which could have improved the stability of the fabricated vessel conduit.

Lastly, we estimated the percentage of area covered by endothelial cells, and surprisingly even when cells migrated along both bilayers, the spreading was superior for PHB/HA-MA ($\approx 70\%$) compared to PCL/HA-MA ($\approx 50\%$) (Figure 7c). The inherent nature of PHB could explain this behavior. In tissue engineering, PHB has been widely studied using different cell lines.^{[15][17]-[19]} It has been determined that different extracellular environments with superior biocompatibility could be easily obtained with essential properties for cell adhesion, viability, and differentiation. Thereafter, we can conclude that PHB/HA-MA self-actuating bilayers depicted high shape tunability, and more outstanding cell biocompatibility, leading to the fabrication of stable grafts with promising properties for substituting damaged vessels conduits.

3. Conclusion

This study reports the fabrication of electrospun self-rolling bilayers that produce stable and easily handleable tubular structures that can be used for blood vessel reconstruction. We compared two kinds of bilayers based on soft thermoplastic polymer (PCL, polycaprolactone) and hard thermoplastic polymer (PHB, polyhydroxybutyrate). Multi-scroll structures with tunable shape and stability in and out of aqueous media were obtained after the shape transformation of the bilayer, whereas PCL-based bilayer rolled longitudinally and PHB-based one rolled transversely concerning the fiber direction. A combination of higher elastic modulus and transverse orientation of fibers with respect to rolling direction allowed precise temporal control of shape transformation of PHB-bilayer – stress produced by swollen HA-MA did not relax with time, and bilayers folding was not affected by the fact that it was fixed in an unfolded state in cell culture medium for more than 1 h. This property of the PHB-bilayer allowed cell culturing without a negative effect on its shape transformation ability. Moreover, the PHB-based tubular structure demonstrated excellent mechanical stability and did not collapse during manipulation that happened to the widely used PCL-based one. Additionally, PHB/HA-MA bilayers showed superior biocompatibility, degradability, and stability compared to PCL/HA-MA. After 14 days of cultivation, our vascular grafts showed high stability in cultivation, and between 50–70% of the area was fully covered. We expect that self-folding bilayers composed of PHB, and HA-MA resemble a suitable environment for fully reendothelialization. All these make a bilayer of transversely aligned hard thermoplastic polymer fibers (such as PHB) and swelling hydrophilic polymer fibers (such as HA-MA) suitable for the fabrication of blood vessel replacement.

4. Experimental Section

Materials: Polycaprolactone (PCL) (80 kDa, Sigma–Aldrich), Poly [(R)-3-hydroxybutyric acid] (PHB) (Sigma–Aldrich), Hyaluronic acid sodium salt (HA) (MW = 1–2 Million Da, Carbosynth Limited), Pluronic F-127 (Sigma–Aldrich), Poly (ethylene oxide) (PEO) (MW = 1 Million g mol⁻¹, Polysciences, Inc.), Alginate sodium salt (Carl Roth GmbH), 2-Hydroxy-4'-(2-hydroxyethoxy)-2-methylpropionophenone (Irgacure D2959) (Sigma–Aldrich), Calcium chloride dihydrate (Sigma–Aldrich), Chloroform (Mw = 119,38 g mol⁻¹, Sigma–Aldrich), Methacrylic anhydride (MA) (Sigma–Aldrich), Sodium Hydroxide (NaOH) (VWR Chemicals), Ethanol 99% (EtOH) (Merk KGaA), Dulbecco's phosphate buffered saline (DPBS) (Sigma–Aldrich), Triton X-100 (Sigma–Aldrich), Calcein-AM (Invitrogen), Ethidium homodimer-1 (EthD-1) (Invitrogen), Fetal bovine serum (FBS) (Gibco), DyLightTM 488 Phalloidin (Cell Signaling Technology), 4',6-diamidino-2-phenylindole (DAPI) (AppliChem), Human umbilical vein endothelial cells (HUVECs) (InSCREENeX GmbH), HUVECs Medium (InSCREENeX GmbH), Penicillin Streptomycin (Pen/Strep) (Gibco), Collagen IV (Merk KGaA), Alamar BlueTM HS Cell Viability Reagent (AB) (Thermo Fisher Scientific).

Synthesis of HA-MA: HA was methacrylated according to the protocol described by Smeds et al.^[58] Initially, a 20-fold excess of MA was dropwise added to a 2% HA solution. The pH of the reaction was several times corrected to 8 with 5 M NaOH. The reaction was then incubated at 5 °C for 24 h under constant stirring. Next, unreacted methacrylic groups were removed against Milli-Q water under dialysis for a week at 37 °C using dialysis tubes (MW = 12–14 kDa) with a pore diameter of 2.5 Å. HA-MA was frozen at –80 °C for ≈ 24 h and subsequently lyophilized for a week using the freeze dryer Freezone 2.5 (Labconco, USA).

Electrospinning: A custom-made electrospinning device (EUB 835, Germany) was utilized for fiber formation. The device consists of two multi-syringe pump systems and two high voltage sources (0–30 kV). Flow rates were set at 0.6 mL h⁻¹, 1 mL h⁻¹, and 0.36 mL h⁻¹ for PCL, PHB, and HA-MA spinning, respectively. Stainless steel needles with an inner diameter of 0.8 mm were chosen for solution spinning, whilst voltages at 15, 20, and 28 kV were applied to the tip of the needle for PCL, PHB, and HA-MA correspondingly. PCL and PHB fibers were collected on top of an ultra-high-speed rotating drum at 6000 and 3000 rpm, whereas HA-MA fibers were collected at 200 rpm. The distance between the dynamic collector and the needles was fixed at 15 cm. Bilayers were fabricated by initial deposition of either PCL (9 wt.%) or PHB (15 wt.%) solutions at a higher speed and subsequent sluggish collection of 2 wt.% HA-MA solution containing 0.1% (w/v) of Irgacure D2959. Due to poor spinnability, HA-MA solution was mixed with 5 wt.% PEO and 20 wt.% Pluronic F127. The final weight ratio used for spinning was 39/26/35 (HA-MA/PEO/Pluronic F127). Finally, electrospun bilayers were crosslinked for 15 min under UV light (VL-125, 8 W/cm², France) using a wavelength of 254 nm at approximately 1 cm. The mat thicknesses were ranging from 30 to 250 μm; we produced mats with different thicknesses to validate the best ratio between both materials in order to fabricate a stable multi-tubular scaffold. ImageJ was used to evaluate the degree of fiber alignment.

Rheological Measurements: The rheological behavior of spinning solutions was investigated using a shear ramp mode with a 0.1 to 100 s⁻¹ at 25 °C using an Anton Paar MCR 702 Rheometer (Anton Paar, Austria).

Scanning Electron Microscopy (SEM): Field emission SEM (Thermo Scientific, Germany) was used to ascertain morphology, diameter, and degree of alignment of electrospun fibers. Therefore, to improve conductivity, samples were coated with ≈2 nm of platinum (Pt) using a Leica EM ACE600 sputter coater (Leica Microsystems, Germany).

Contact Angle (CA): Static contact angle measurements were performed by adding a drop of ultra-pure Milli-Q water on three different points on top of a silicon wafer coated with PCL and PHB polymer solution using a KRÜSS drop shape analyzer (KRÜSS DSA25E GmbH, Germany). Advancing and receding contact angle (CA) measurements were used to estimate the wetting properties of electrospun PCL and PHB mats. Therefore, CA hysteresis was studied by adding an ultrapure drop of 5 μL of Milli-Q water on top of the mats for ≈10 s. For advancing volume studies, the volume was sequentially increased up to 25 μL, 5 μL each time with a rate of 2.67 μL s⁻¹, and vice versa during receding volume analysis. All measurements were made at room temperature.

Differential scanning calorimetry (DSC): Thermo-responsive behavior of electrospun PCL and PHB fibers was checked under DSC measurements (Mettler Toledo DSC3, Switzerland). Initially, ≈5–7 mg of electrospun fibers were loaded in aluminum crucibles. Subsequently, both polymers were subjected to three steps: (1) heat step from –10 to 200 °C, (2) cooling to –10 °C, and finally (3) new heating up to 200 °C. For both polymers, the heating/cooling rate was fixed at 10 K min⁻¹.

Mechanical Testing: Mechanics of electrospun mono and bilayers were checked using dynamic mechanical analysis (DMA) (Anton Paar MCR 702e, Austria). Dimensions for samples were fixed at 35 × 10 mm². Thickness was measured under SEM to avoid discrepancy.

Tensile Testing: Tensile tests were conducted on both dry and wet states. Therefore, rectangular strips were vertically held using a solid rectangular fixture (SRF LD/TS Anton Paar, Austria), and the lower motor was displaced ≈9 mm downwards. The sample was clamped and fully extended to avoid artifacts. Subsequently, dry samples were extended until there was an evident deformation or rupture. Next, the second round of rectangular samples fully soaked within an immersion cell (Anton Paar, Austria) with DPBS was tested using the same parameters as previously described.

DMA: Samples with the same dimensions as previously described were also subjected to amplitude sweep measurements at room temperature (RT). Static forces of 450 and 800 mN and dynamic forces of 10–100 mN and 50–750 mN were added to PCL and PHB mono and bilayers, respectively. Frequency was kept constant at 1 Hz, whilst relative humidity (RH) was increased from 5 up to 90%.

Furthermore, electrospun bilayers were subjected to a temperature-humidity sweep test. Herein, static forces at 450 and 800 mN and dynamic

forces at 100 and 30 mN were set for PCL/HA-MA and PHB/HA-MA bilayers, respectively. Frequency was fixed at 1 Hz, and RH was sequentially increasing from 5 up to 90% with a 2%/min rate. Simultaneously, the temperature rose from 20 up to 40 °C under a 1°C min⁻¹ rate.

Degradation Studies: Electrospun mats and folded PCL/HA-MA and PHB/HA-MA bilayers were subjected to real-time degradation tests for 4 weeks in DPBS at 37 °C. Mats were removed at different time points: 1, 2, 3, and 4th weeks. Weight, tube diameter, and morphology were investigated.

Cell Culture Studies: HUVECs with a passage of less than six were seeded on top of highly aligned PCL and PHB fibers, PCL/HA-MA, and PHB/HA-MA bilayers. Cell studies were performed using two different experiments. In the first of them, mono- and bi-nanofibrous scaffolds were gripped on cell crown inserts (Scaffdex CellCrown™). Whereas in the second one, entrapment of cells was studied upon folding of bilayers. Scaffolds were incubated at RT with 70% EtOH for ≈1 h and later sterilized under UV light for 30 min. To improve HUVECs adhesion, scaffolds were coated with sterile collagen IV solution in DPBS (1:4) for 30 min at RT. Cell densities of 7000 cells cm⁻² and 100 000 cells cm⁻² were used for metabolic activity, cell viability, and cell distribution tests, respectively. Cells were grown using HUVECs medium, containing basal medium and supplements, 10% v/v FBS and 1% v/v Pen/Stre according to protocol described by the manufacturer (InSCREENeX GmbH). HUVECs media was refreshed every two days to provide cells with enough amount of nutrients.

Metabolic Activity: Cell proliferation was ascertained using alamar blue (AB) assay at different time points: 1, 4, and 7 days. AB solution was prepared according to protocol described by the manufacturer (Thermo Fischer Scientific) in a ratio of 10% v/v with HUVECs medium. Subsequently, 500 μL of AB was added to scaffolds within the crowns and incubated at 37 °C for ≈3 h. Each 30 min, the well-plates were shaken back and forth to avoid gradient formation. After incubation, the solution was transferred to eppendorfs and kept under ice-cold conditions to stop the reaction. Then, 100 μL of aliquots were transferred onto a 96-well plate, and fluorescence was measured at 530 nm excitation and 590 nm emission utilizing a multimode reader (BertholdTech TriStar2s, Germany). A positive control using reduced AB and negative control with only AB in media were used to avoid false-positive signal formation.

Live/dead Assay: The viability of HUVECs cultured on electrospun scaffolds (PCL, PHB, and PCL/HA-MA and PHB/HA-MA bilayers) was determined after 7 days using live/dead assay. Thereby, samples were incubated for 30 min at RT using a DPBS staining solution containing 3.6 μL of Calcein-AM and 4 μL of EtD-1. Cell viability was then calculated by measuring the number of dead and live cells in 6 different images obtained using a fluorescence microscope (Nikon Eclipse Ti2, Japan) and confocal microscope TCS SP8 (Leica DMI8, Germany).

Cell Distribution: Cell distribution along electrospun scaffolds was studied by cultivating 100 000 cells cm⁻² on top of collagen-coated mats. HUVECs medium was replaced every two days. Scaffolds were stained using DAPI (nucleus) and phalloidin (actin filaments) staining after cultivation for 4, 7, and 14 days. Hence, samples were initially rinsed twice using sterile DPBS; then fixation was performed for 15 min at RT using 3.7% formaldehyde. Next, samples were newly washed twice with DPBS, and the cell membrane was permeabilized by incubating scaffolds with 0.1% Triton for 5 min at RT. Subsequently, mats were washed with DPBS and incubated with a staining solution of 2 mL DPBS containing 2 μL DAPI and 50 μL of phalloidin for 30 min at RT. After staining, samples were one last time rinsed with DPBS, and images were obtained using confocal microscopy TCS SP8 (Leica DMI8, Germany). According to the protocol discussed by Aubin et al.,^[59] the nuclei orientation was estimated using a plug-in for alignment analysis. The percentage of the coverage area was also estimated through the threshold option in image j.

Fabrication of Vascular Scaffold: Entrapment of HUVECs along PCL/HA-MA and PHB/HA-MA bilayers was studied using DAPI and phalloidin staining. Therefore, a cell density of 100 000 cells/cm² was seeded on top of sterile collagen-coated bilayers. To prevent folding upon swelling, bilayers were physically restricted with Teflon rings to allow proper cell adhesion for 30 min at 37 °C. Subsequently, rings were removed, and bilayers formed scroll-like tubes. Cells were left to grow for 14 days at 37 °C within the incubator before staining. Vascular grafts were imaged using

fluorescence and confocal microscope, and the coverage area was determined using image j.

Statistical Analysis: Standard deviation was stated as \pm , and 2–6 replicates were used in each test. One and two-way analysis of variance (ANOVA) and Tukey's test were conducted using Origin Software to determine any differences among the studied samples. A value of $p < 0.05$ was considered significant.

Supporting Information

Supporting Information is available from the Wiley Online Library or from the author.

Acknowledgements

The manuscript was written with the contributions of all authors. All authors have given approval to the final version of the manuscript. The authors declare that Anton Paar develops, produces, and sells the rheometer MCR 702 and the rheometer MCR 702e MultiDrive. J.A.R.A. is an employee of Anton Paar. This work was supported by DFG (Grant No. IO 68/17-1, IO 68/14-1). The authors would further like to thank Prof. Scheibel for providing the access to SEM and confocal microscope.

Open Access funding enabled and organized by Projekt DEAL.

Conflict of Interest

The authors declare no conflict of interest.

Data Availability Statement

The data that support the findings of this study are available from the corresponding author upon reasonable request.

Keywords

electrospun bilayer, fibrous scaffolds, self-folding, vascular graft

Received: August 1, 2022

Revised: September 11, 2022

Published online: October 28, 2022

- [1] L. Xue, H. P. Greisler, *J Vasc Surg Venous Lymphat Disord* **2003**, *37*, 472.
- [2] E. T. Lee, B. V. Howard, W. Wang, T. K. Welty, J. M. Galloway, L. G. Best, R. R. Fabsitz, Y. Zhang, J. Yeh, R. B. Devereux, *Circulation* **2006**, *113*, 2897.
- [3] E. S. Ford, U. A. Ajani, J. B. Croft, J. A. Critchley, D. R. Labarthe, T. E. Kottke, W. H. Giles, S. Capewell, *N. Engl. J. Med.* **2007**, *356*, 2388.
- [4] J. F. Chester, *Ann. Coll. Surg. Hong Kong* **2002**, *6*, 97.
- [5] M. R. De Vries, K. H. Simons, J. W. Jukema, J. Braun, P. H. A. Quax, *Nat Rev Cardiol* **2016**, *13*, 451.
- [6] A. J. Melchiorri, N. Hibino, C. A. Best, T. Yi, Y. U. Lee, C. A. Kraynak, L. K. Kimerer, A. Krieger, P. Kim, C. K. Breuer, J. P. Fisher, *Adv. Healthcare Mater.* **2016**, *5*, 319.
- [7] Z. Sun, *Anatol J Cardiol* **2017**, *17*, 423.
- [8] D. J. Wu, K. Van Dongen, W. Szymczyk, P. J. Besseling, R. M. Cardinaels, G. Marchioli, M. H. P. Van Genderen, C. V. C. Bouten, A. I. P. M. Smits, P. Y. W. Dankers, *Front. Mater.* **2020**, *7*, 1.
- [9] T. Baltazar, J. Merola, C. Catarino, C. B. Xie, N. C. Kirkiles-Smith, V. Lee, S. Hotta, G. Dai, X. Xu, F. C. Ferreira, W. M. Saltzman, J. S. Pober, P. Karande, *Tissue Eng., Part A* **2020**, *26*, 227.
- [10] D. Richards, J. Jia, M. Yost, R. Markwald, Y. Mei, *Ann. Biomed. Eng.* **2017**, *45*, 132.
- [11] G. Gao, H. Kim, B. S. Kim, J. S. Kong, J. Y. Lee, B. W. Park, S. Chae, J. Kim, K. Ban, J. Jang, H. J. Park, D.-W. Cho, *Appl. Phys. Rev.* **2019**, *6*, 041402.
- [12] B. Duan, *Ann. Biomed. Eng.* **2017**, *45*, 195.
- [13] L. Ionov, *Adv. Healthcare Mater.* **2018**, *7*, 1800412.
- [14] L. Ye, J. Cao, L. Chen, X. Geng, A.-Y. Zhang, L.-R. Guo, Y.-Q. Gu, Z.-G. Feng, *J. Biomed. Mater. Res., Part A* **2015**, *103*, 3863.
- [15] L. Soletti, Y. Hong, J. Guan, J. J. Stankus, M. S. El-Kurdi, W. R. Wagner, D. A. Vorp, *Acta Biomater.* **2010**, *6*, 110.
- [16] S. F. Karkan, S. Davaran, R. Rahbarghazi, R. Salehi, A. Akbarzadeh, *J. Biol. Eng.* **2019**, *13*, 83.
- [17] S. Cheng, Y. Jin, N. Wang, F. Cao, W. Zhang, W. Bai, W. Zheng, X. Jiang, *Adv. Mater.* **2017**, *29*, 1700171.
- [18] P. Xiang, M. Li, C.-Y. Zhang, D.-L. Chen, Z.-H. Zhou, *Int. J. Biol. Macromol.* **2011**, *49*, 281.
- [19] S. Haghjooy Javanmard, J. Anari, A. Zargar Kharazi, E. Vatankhah, *J. Biomater. Appl.* **2016**, *31*, 438.
- [20] Y. Zhang, L. Ionov, *Langmuir* **2015**, *31*, 4552.
- [21] I. Apsite, G. Stoychev, W. Zhang, D. Jehnichen, J. Xie, L. Ionov, *Biomacromolecules* **2017**, *18*, 3178.
- [22] A. Rafsanjani, V. Brulé, T. L. Western, D. Pasini, *Sci. Rep.* **2015**, *5*, 8064.
- [23] J. Fouchard, T. P. J. Wyatt, A. Proag, A. Lisica, N. Khalilgharibi, P. Recho, M. Suzanne, A. Kabla, G. Charras, *Proc. Natl. Acad. Sci. USA* **2020**, *117*, 9377.
- [24] L. Zhang, Y. Xiang, H. Zhang, L. Cheng, X. Mao, N. An, L. Zhang, J. Zhou, L. Deng, Y. Zhang, X. Sun, H.ã©L. A. Santos, W. Cui, *Adv. Sci.* **2020**, *7*, 1903553.
- [25] A. Kirillova, R. Maxson, G. Stoychev, C. T. Gomillion, L. Ionov, *Adv. Mater.* **2017**, *29*, 1703443.
- [26] B. Yuan, Y. Jin, Y. Sun, D. Wang, J. Sun, Z. Wang, W. Zhang, X. Jiang, *Adv. Mater.* **2012**, *24*, 890.
- [27] M. Rampichová, E. KošťÁková Kuželová, E. Filová, J. Chvojka, J. Šafka, M. Pelcl, J. Daňková, E. Prosecká, M. Buzgo, M. Plencner, D. Lukáš, E. Amler, *Cell. Adhes. Migr.* **2018**, *12*, 271.
- [28] S. Jiang, F. Liu, A. Lerch, L. Ionov, S. Agarwal, *Adv. Mater.* **2015**, *27*, 4865.
- [29] I. Apsite, J. M. Uribe, A. F. Posada, S. Rosenfeldt, S. Salehi, L. Ionov, *Biofabrication* **2019**, *12*, 015016.
- [30] I. Apsite, G. Constante, M. Dulle, L. Vogt, A. Caspari, A. R. Boccaccini, A. Synytska, S. Salehi, L. Ionov, *Biofabrication* **2020**, *12*, 035027.
- [31] K. Sombatmankhong, O. Suwanton, S. Waleetorncheepsawat, P. Supaphol, *J. Polym. Sci., Part. B: Polym. Phys.* **2006**, *44*, 2923.
- [32] N. Nagiah, L. Madhavi, R. Anitha, N. T. Srinivasan, U. T. Sivagnanam, *Polym. Bull.* **2013**, *70*, 2337.
- [33] O. Suwanton, S. Waleetorncheepsawat, N. Sanchavanakit, P. Pavasant, P. Cheepsunthorn, T. Bunaprasert, P. Supaphol, *Int. J. Biol. Macromol.* **2007**, *40*, 217.
- [34] V. Kundrat, N. Cernekova, A. Kovalcik, V. Enev, I. Marova, *Materials* **2019**, *12*, 1924.
- [35] S. Y. Chan, B. Q. Y. Chan, Z. Liu, B. H. Parikh, K. Zhang, Q. Lin, X. Su, D. Kai, W. S. Choo, D. J. Young, X. J. Loh, *ACS Omega* **2017**, *2*, 8959.
- [36] M. Labet, W. Thielemans, *Chem. Soc. Rev.* **2009**, *38*, 3484.
- [37] P. Kampeerappun, *J. Appl. Polym. Sci.* **2016**, *133*, n/a.
- [38] G. Constante, I. Apsite, H. Alkhamis, M. Dulle, M. Schwarzer, A. Caspari, A. Synytska, S. Salehi, L. Ionov, *ACS Appl. Mater. Interfaces* **2021**, *13*, 12767.
- [39] D. Daranarong, R. T. H. Chan, N. S. Wanandy, R. Molloy, W. Punyodom, L. J. R. Foster, *Biomed Res. Int.* **2014**, *2014*, id741408.
- [40] Q. Wu, Y. Wang, G.-Q. Chen, *Artif Cells Blood Substit Immobil Biotechnol* **2009**, *37*, 1.

- [41] G. Barouti, C. G. Jaffredo, S. M. Guillaume, *Prog. Polym. Sci.* **2017**, *73*, 1.
- [42] A. Fakhari, C. Berkland, *Acta Biomater.* **2013**, *9*, 7081.
- [43] E. López-Ruiz, G. Jiménez, L. Álvarez De Cienfuegos, C. Antich, R. Sabata, J. Marcha, P. Gálvez-Martín, *Eur Cell Mater* **2019**, *37*, 186.
- [44] A. De Pieri, Y. Rochev, D. I. Zeugolis, *NPJ Regen Med* **2021**, *6*, 18.
- [45] E. Masaeli, M. Morshed, M. H. Nasr-Esfahani, S. Sadri, J. Hilderink, A. Van Apeldoorn, C. A. Van Blitterswijk, L. Moroni, *PLoS One* **2013**, *8*, e57157.
- [46] L. R. Lizarraga-Valderrama, C. S. Taylor, F. Claeysens, J. W. Haycock, J. C. Knowles, I. Roy, *J Tissue Eng Regen Med* **2019**, *13*, 1581.
- [47] D. M. Correia, C. Ribeiro, J. C. C. Ferreira, G. Botelho, J. L. G. Ribelles, S. Lancers-Méndez, V. Sencadas, *Polym. Eng. Sci.* **2014**, *54*, 1608.
- [48] I. Yoshihiro, H. Hirokazu, M. Kamitakahara, C. Ohtsuki, M. Tanihara, I.-K. Kang, O. H. Kwon, *J. Biosci. Bioeng.* **2005**, *100*, 43.
- [49] A. Köwitsch, Y. Yang, N. Ma, J. Kuntsche, K. Mäder, T. Groth, *Biotechnol, Appl. Biochem.* **2011**, *58*, 376.
- [50] S. Timoshenko, *J. Opt. Soc. Am.* **1925**, *11*, 233.
- [51] F. Viñals, J. Pouysségur, *Mol. Cell. Biol.* **1999**, *19*, 2763.
- [52] R. Daum, D. Visser, C. Wild, L. Kutuzova, M. Schneider, G. Lorenz, M. Weiss, S. Hinderer, U. A. Stock, M. Seifert, K. Schenke-Layland, *Cells* **2020**, *9*, 778.
- [53] M. Toshmatova, S. Nakanishi, Y. Sugimura, V. Schmidt, A. Lichtenberg, A. Assmann, P. Akhyari, *Materials* **2019**, *12*, 3351.
- [54] M. Murga, O. Fernandez-Capetillo, G. Tosato, *Am. J. Blood Res.* **2005**, *105*, 1992.
- [55] R. J. Smith, B. Nasiri, J. Kann, D. Yergeau, J. E. Bard, D. D. Swartz, S. T. Andreadis, *Nat. Commun.* **2020**, *11*, 1622.
- [56] J. P. Hytönen, O. Leppänen, J. Taavitsainen, P. Korpisalo, S. Laidinen, K. Alitalo, J. Wadström, T. T. Rissanen, S. Ylä-Herttuala, *Vasc. Biol.* **2019**, *1*, 1.
- [57] O. Kérourédan, J.-M. Bourget, M. Rémy, S. Crauste-Manciet, J. Kalisky, S. Catros, N. B. Thébaud, R. Devillard, *J Mater Sci Mater Med* **2019**, *30*, 28.
- [58] K. A. Smeds, M. W. Grinstaff, *J Biomed Mater Res* **2001**, *54*, 115.
- [59] H. Aubin, J. W. Nichol, C. B. Hutson, H. Bae, A. L. Sieminski, D. M. Crokek, P. Akhyari, A. Khademhosseini, *Biomaterials* **2010**, *31*, 6941.